Supplementary Information for "The stop-start control of seismicity by fault bends along the Main Himalayan Thrust"

Sharadha Sathiakumar and Sylvain Barbot

Contents of this file

1. Supplementary Figures 1 to 5
2. Supplementary Tables 1 and 2

Parameter	Symbol	Value
Effective normal stress	$\bar{\sigma}$	$50\,\mathrm{MPa}$
Reference velocity	V_0	$10^{-6}\,\mathrm{m/s}$
Rigidity	G	$30\,\mathrm{GPa}$
Poisson's ratio	ν	0.25
Shear wave speed	V_s	$3 \times 10^3\,\mathrm{m/s}$
Loading rate	V_L	$20\,\mathrm{mm/yr}$
Steady-state rate dependence in velocity-strengthening region	$a-b$	$+1 \times 10^{-2}$
Steady-state rate dependence in velocity-weakening region	$a-b$	-4×10^{-3}
Characteristic weakening distance	L	$0.01 - 2\,\mathrm{m}$
Down-dip width of the velocity-weakening region for model H	W	$92\,\mathrm{km}$
Down-dip width of the velocity-weakening region for model E	W	$89.58\,\mathrm{km}$
Model H		
Dieterich-Ruina-Rice number	R_u	$0.3 - 61.3$
Non-dimensional parameter	R_b	0.2
Model E		
Dieterich-Ruina-Rice number	R_u	$0.3 - 59.7$
Non-dimensional parameter	R_b	0.2

Supplementary Table 1: **Summary of frictional parameters that explore the non-dimensional parameter R_u at fixed $R_b = 0.2$.** Frictional parameters and its values using model E and model H sub-surface fault geometry in the simulations presented in Supplementary Figure 2. The static friction coefficient, reference velocity, shear wave speed, and Poisson's ratio are the same for all simulations. We vary the characteristic weakening distance L for simulations that explore a range of non-dimensional parameters R_u. The down-dip width of the velocity-weakening region for geometry E and H is fixed for all simulations such that the depth of the transition zone is at $\sim 15\,\mathrm{km}$.

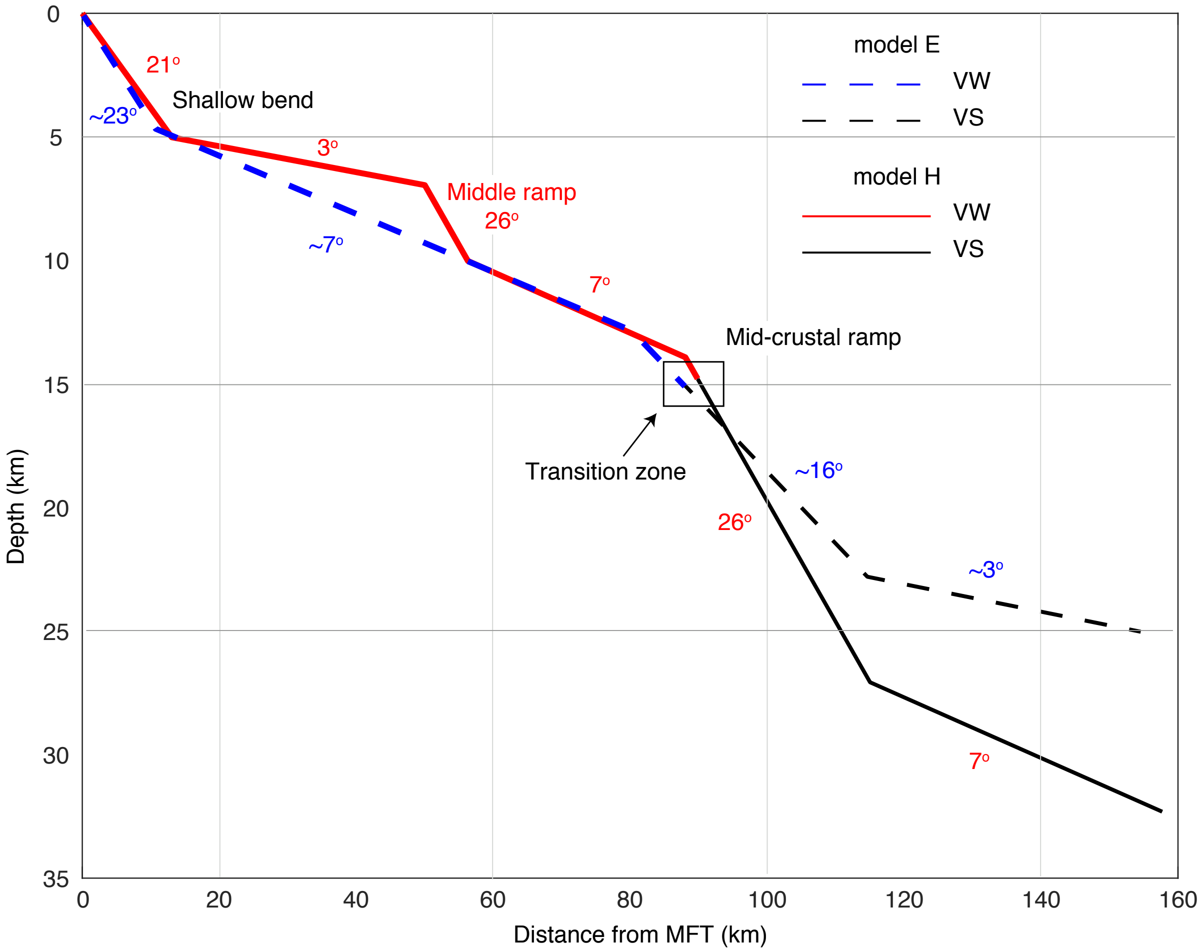

Supplementary Figure 1: **Two-dimensional fault geometry models E and H.** The fault geometry along a representative cross-section perpendicular to the plate boundary that crosses the Gorkha-Pokhara Anticlinorium in the middle of the Gorkha coseismic rupture. The dip angles of the individual fault segments are marked for model E (blue) and model H (red). The transition zone of both models is located between 80 and 100 km from the surface trace of MFT (Main Frontal Thrust). The depth of the transition zone is about 15 km in both models. Both the shallow bend and the mid-crustal ramps have similar dip angles and are present at comparable depths. The main difference in fault structure between the two models is in the middle of the seismogenic zone: model E has a single décollement that connects the shallow bend to the mid-crustal ramp in comparison to the more complex fault structure with a middle ramp in model H.

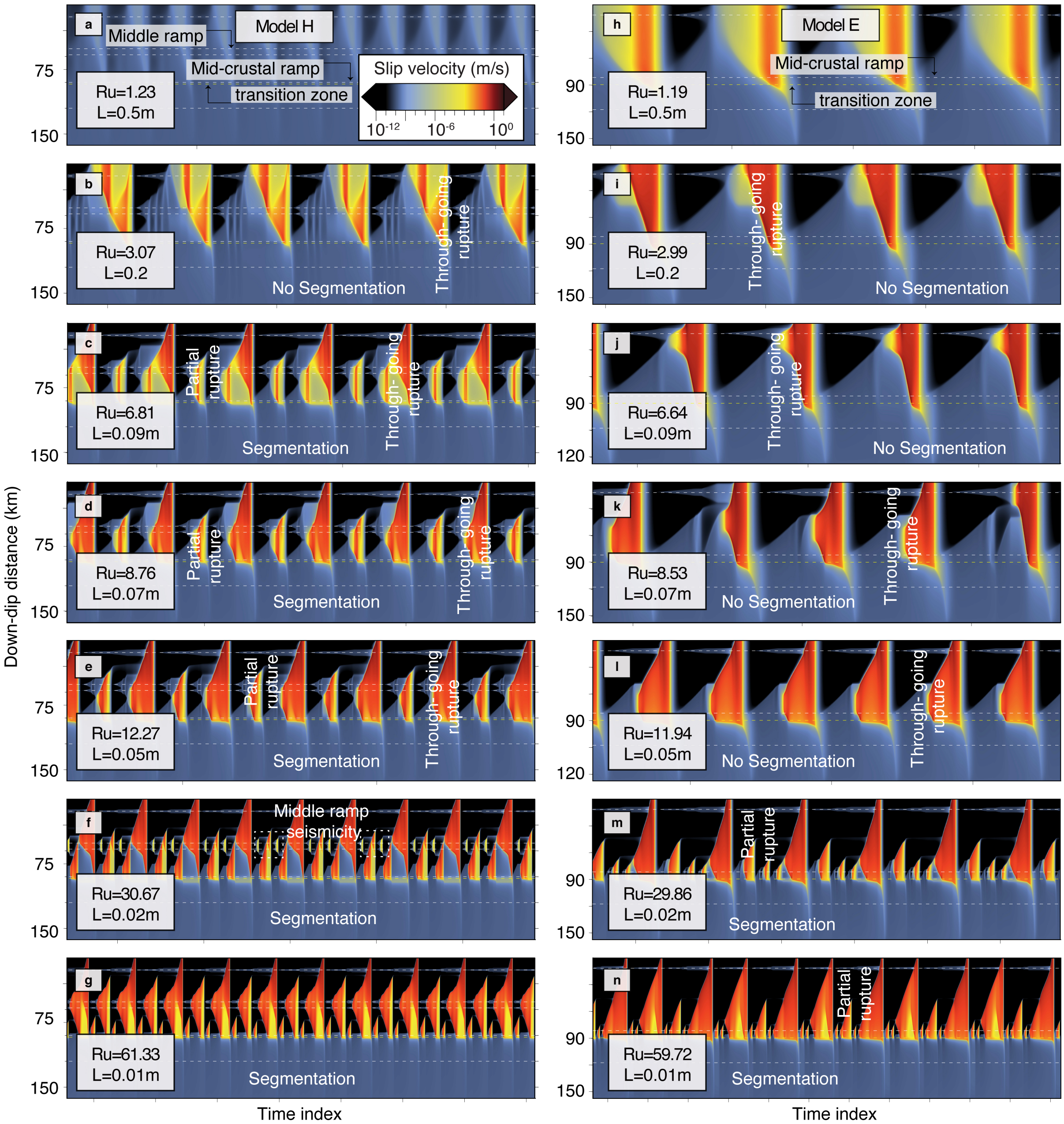

Supplementary Figure 2: **Earthquake cycle dynamics exploring a large range of R_u values.** a-n) Simulation results for model H (left column) and model E (right column). The dotted white lines indicate the position of the fault bends and the transition zone that represent areas of high stress concentrations. The colour indicates the fault slip rate; red represents seismic velocities and dark blue represents fault locking. The slip-weakening distance L ranges between 0.5 m to 0.01 m which results in R_u values to range between 1 and 60. The x axis in the plots show time steps rather than time itself, which is non-uniformly spaced such that fast events have a finer resolution than during interseismic periods. As R_u increases, slip complexity increases for both geometry models. The frictional parameters are listed in Supplementary Table 1.

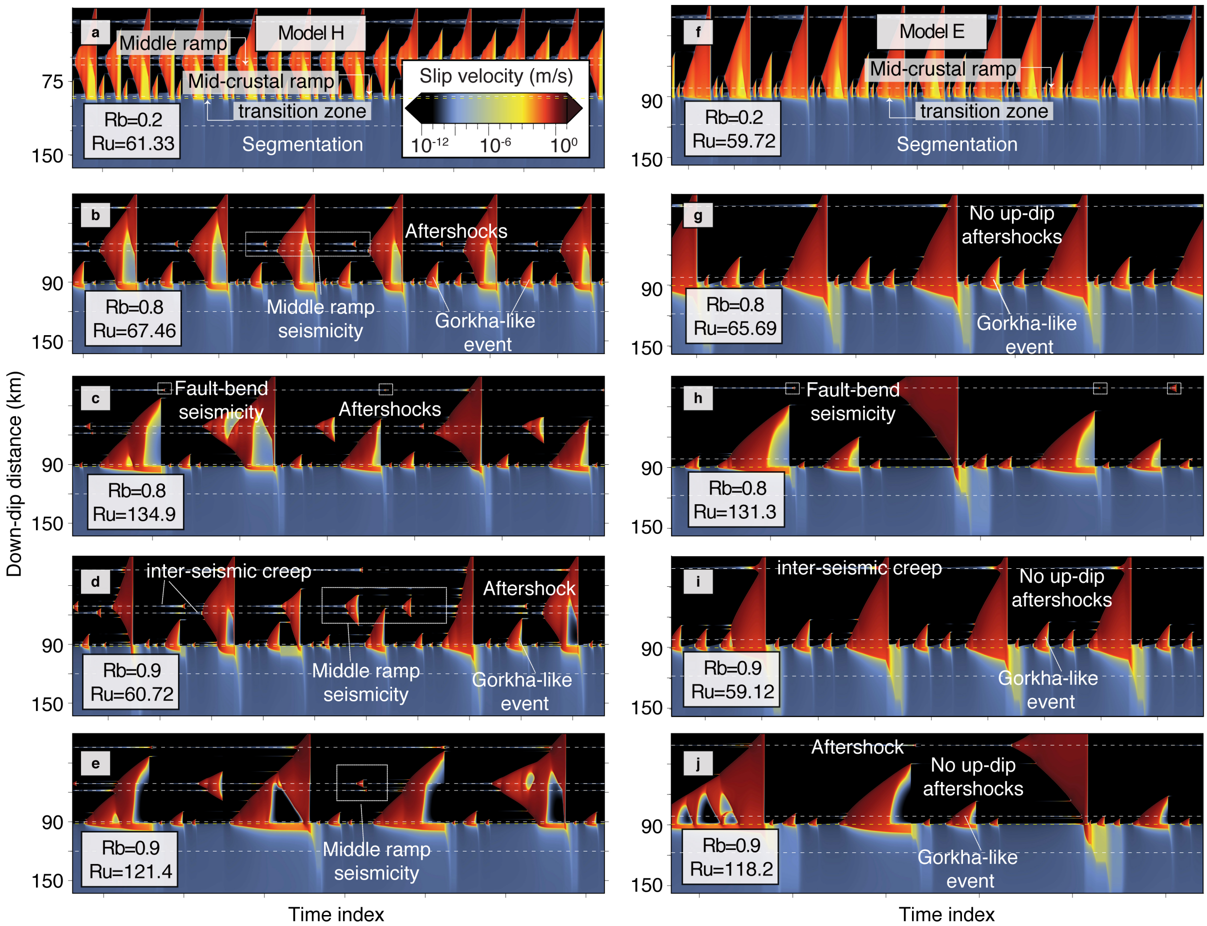

Supplementary Figure 3: **Earthquake cycle dynamics exploring R_b values.** a-j) Simulation results for model H (left column) and model E (right column). The dotted white lines indicate the position of the fault bends and the transition zone that represent areas of high stress concentrations. The colour indicates the fault slip rate; red represents seismic velocities and dark blue represents fault locking. The friction parameters a, b, L are varied to explore the $R_u - R_b$ phase space. The x-axis in the plots show time steps rather than time itself, which is non-uniformly spaced such that fast events have a finer resolution than during interseismic periods. As R_b increases, pulse-like ruptures and fault bend seismicity increases. The frictional parameters are listed in Supplementary Table 2.

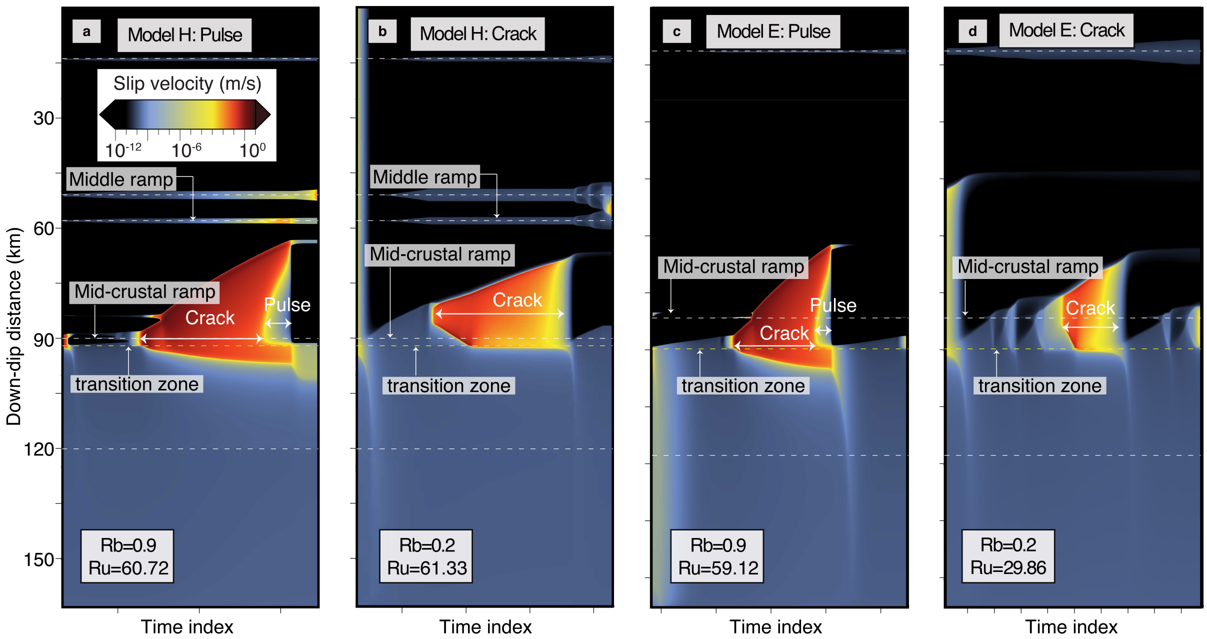

Supplementary Figure 4: **Pulse-like vs crack-like rupture propagation.** With higher $R_b = 0.9$ values, the rupture transitions from crack-like to pulse like with both model E and model H (a and c). In contrast, with lower values of $R_b = 0.2$, the rupture is fully crack-like (b and d). The colour indicates the fault slip rate; red represents seismic velocities and dark blue represents fault locking. The x axis in the plots show time steps rather than time itself, which is nonuniformly spaced such that fast events have a finer resolution than during interseismic periods.

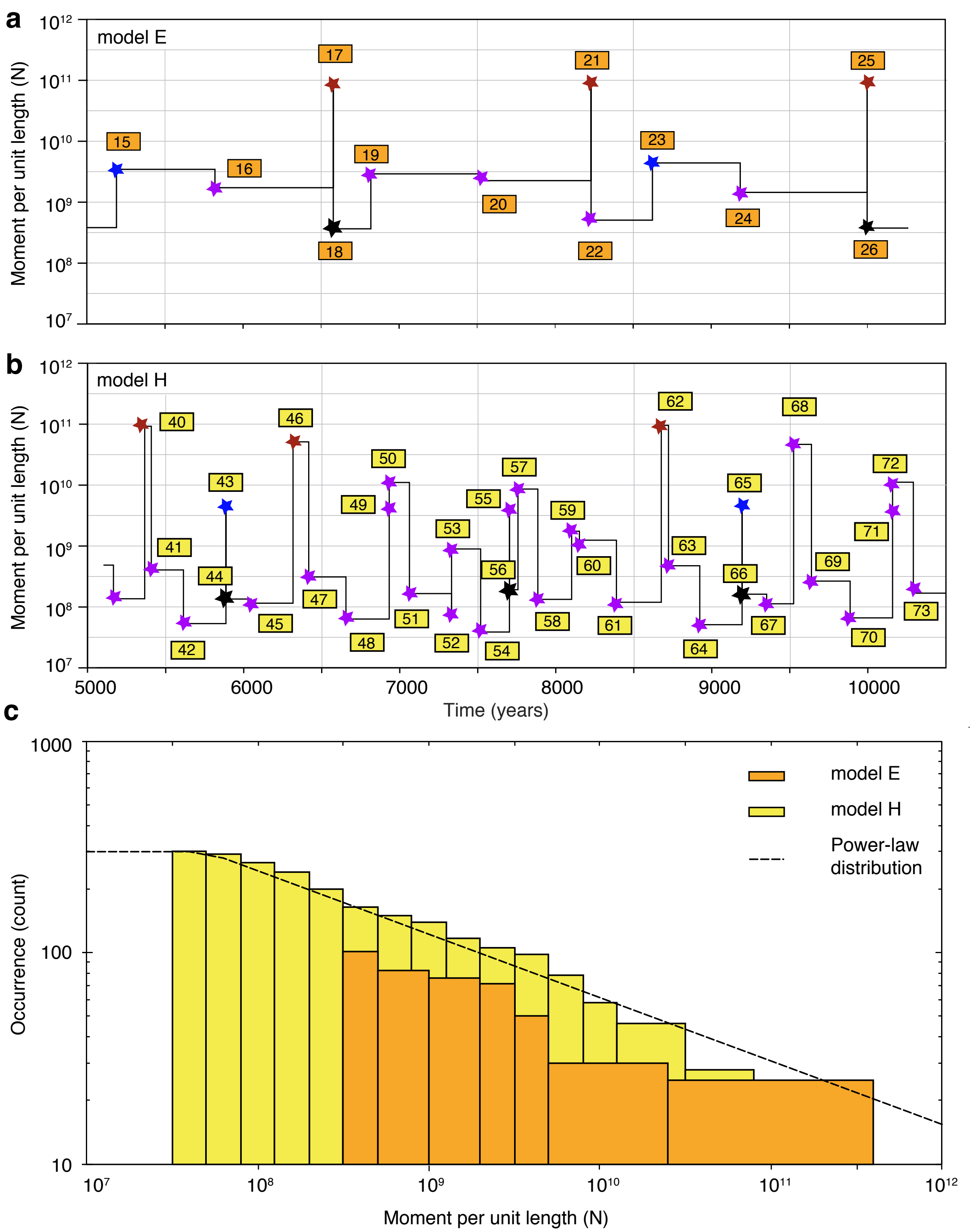

Supplementary Figure 5: **Statistical properties of simulated events using the two end-member geometry models.** Simulation results computed for 5,000 years for a) model E and b) model H, showing giant surface ruptures (red stars), partial ruptures of varying sizes (purple stars), Gorkha-like events (blue stars), and aftershocks (black stars) with varying magnitudes (cumulative force in 2-D). c) Cumulative histogram of all events for a catalogue spanning 45,000 years for both geometries. Model H approximately follows a power-law distribution indicated by the dashed black line. The Pareto distribution (dashed line) is for a power exponent $\alpha = 0.3$ for moment per unit length above 5×10^7 N.

Parameter	Symbol	Value
Reference velocity	V_0	10^{-6} m/s
Rigidity	G	30 GPa
Poisson's ratio	ν	0.25
Shear wave speed	V_s	3×10^3 m/s
Loading rate	V_L	20 mm/yr
Steady-state rate dependence in velocity-strengthening region	$a-b$	$+1 \times 10^{-2}$
Down-dip width of the velocity-weakening region for model H	W	92 km
Down-dip width of the velocity-weakening region for model E	W	89.58 km
Simulations A and F		
Effective normal stress	$\bar{\sigma}$	50 MPa
Characteristic weakening distance	L	0.01 m
Steady-state rate dependence in velocity-weakening region for $R_b = 0.2$	$a-b$	-4×10^{-3}
Simulations B and G		
Effective normal stress	$\bar{\sigma}$	50 MPa
Characteristic weakening distance	L	0.04 m
Steady-state rate dependence in velocity-weakening region for $R_b = 0.8$	$a-b$	-1.76×10^{-2}
Simulations C and H		
Effective normal stress	$\bar{\sigma}$	100 MPa
Characteristic weakening distance	L	0.04 m
Steady-state rate dependence in velocity-weakening region for $R_b = 0.8$	$a-b$	-1.76×10^{-2}
Simulations D and I		
Effective normal stress	$\bar{\sigma}$	50 MPa
Characteristic weakening distance	L	0.05 m
Steady-state rate dependence in velocity-weakening region for $R_b = 0.9$	$a-b$	-1.98×10^{-2}
Simulations E and J		
Effective normal stress	$\bar{\sigma}$	100 MPa
Characteristic weakening distance	L	0.05 m
Steady-state rate dependence in velocity-weakening region for $R_b = 0.9$	$a-b$	-1.98×10^{-2}

Supplementary Table 2: **Summary of frictional parameters that explore the non-dimensional parameter R_b at fixed R_u.** Frictional parameters and its values using model E and model H subsurface fault geometry in the simulations presented in Supplementary Figure 3. The static friction coefficient, reference velocity, shear wave speed, and Poisson's ratio are the same for all simulations. We vary the effective normal stress, frictional parameters a and b, and characteristic weakening distance L for simulations that explore a range of non-dimensional parameters R_u and R_b. The down-dip width of the velocity weakening region for models E and H is fixed for all simulations, such that the depth of the transition zone is at ~ 15 km.